

Minimum-Time Sequential Traversal by a Team of Small Unmanned Aerial Vehicles in an Unknown Environment with Winds

Jeffrey A. DesRoches¹ and Raghvendra V. Cowlagi¹

Abstract—We consider the problem of transporting multiple packages from an initial location to a destination location in a windy urban environment using a team of SUAVs. Each SUAV carries one package. We assume that the wind field is unknown, but wind speed can be measured by SUAVs during flight. The SUAVs fly sequentially one after the other, measure wind speeds along their trajectories, and report the measurements to a central computer. The overall objective is to minimize the total travel time of all SUAVs, which is in turn related to the number of SUAV traversals through the environment. For a discretized environment modeled by a graph, we describe a method to estimate wind speeds and the time of traversal for each SUAV path. Each SUAV traverses a minimum-time path planned based on the current wind field estimate. We study cases of static and time-varying wind fields with and without measurement noise. For each case, we demonstrate via numerical simulation that the proposed method finds the optimal path after a minimal number of traversals.

I. INTRODUCTION

Urban air mobility promises to revolutionize the transportation of passengers and goods in densely populated areas [1], with envisioned applications in time-sensitive package deliveries [2] and emergency response services [3].

A key challenge in urban air mobility, and especially for small uncrewed aerial vehicles (SUAVs) designed for package delivery, to navigate urban environments is the presence of dynamic wind conditions. Due to the “urban canyon” effect, wind gusts at relatively low altitudes in urban areas can reach speeds as high as 20 m/s [4], which is comparable to – or at least a significant fraction of – the cruise speeds of many SUAVs. Low-altitude urban wind fields are complex and difficult to model, with relatively few datasets and studies of reconstructing the wind field from data, e.g., [5]. Some recent studies report on SUAV path-planning in urban areas using wind data reconstructed with computational fluid dynamics in [6], [7]. However, these are limited to static fields that are assumed to be fully known to the path-planning algorithm.

The problem of SUAV path-planning in dynamic urban wind fields is challenging not merely due to the lack of pre-existing datasets. Even if the typical wind fields in a particular urban area were easily available, these data would not be helpful of the wind fields prevalent during unusual weather patterns or relatively rare natural events such as hurricanes. Furthermore, existing datasets examine the wind field at coarse temporal resolutions (e.g., 10 minutes)

because the timescales considered are typically seasonal or annual [8].

In this paper, we consider the problem of transporting multiple packages from an initial location to a destination location in a windy urban environment using a team of SUAVs. Each SUAV carries one package. The overall objective is to minimize the total travel time of all SUAVs. We assume that the wind field is unknown, but wind speed can be measured by SUAVs during flight along their trajectories. The SUAVs fly one after the other, measure wind speeds along their trajectories, and report the measurements to a central computer, henceforth referred to as the *agent*. The flight of a single SUAV in the team from the initial to the goal location is called a *pass*. The central computer calculates an estimate of the wind field based on measurements collected in each pass and transmits the estimate to all other SUAVs.

A naïve solution to this problem is to make the first one or two SUAVs follow “lawnmower” patterns to fully survey the entire environment. This would enable the remaining SUAVs to plan paths using accurate and precise estimates of the wind field. However, this solution will necessitate a large time of travel by the initial surveying SUAVs. Furthermore, this solution may not be implementable in large environments, where a single SUAV may not have enough range and endurance to survey the environment. Therefore, we seek a solution for planning the path of each SUAV towards the overall objective of minimizing the team’s total travel time.

Typically, the goal of path-planning is to find a path that minimizes some cost function. The most commonly used path-planning methods include cell- or grid-based discretization, probabilistic roadmaps, and artificial potential field techniques [9], [10]. In cell- or grid-based discretization methods, Dijkstra’s algorithm or A* are employed to efficiently compute the shortest path. Other emerging approaches, such as deep reinforcement learning [11], [12] claim to handle complex and uncertain, yet static environments. However, these methods typically large volumes of training data obtained from historical datasets or simulations. This study aims to remove this requirement altogether. Our assumption is that all relevant data regarding the wind field is to be collected during the aforesaid SUAV passes.

Measurements from sensors are noisy and may be intermittently unavailable. Typical estimation techniques such as the Kalman filter [13], maximum likelihood estimator [14], and Bayesian filter [15] are all well studied estimators for linear systems. The extended Kalman filter, unscented Kalman filter [16] and the particle filter [17] are common for nonlinear dynamical systems. The common underlying

¹Jeffrey A. DesRoches and Raghvendra V. Cowlagi are with the Department of Aerospace Engineering, Worcester Polytechnic Institute, Worcester, MA 01609. Email: jadesroches, rvcowlagi@wp1.edu

assumption for these estimators is the presence of a model of the system’s evolution as well as a measurement model. If the system model is unknown or highly imprecise (i.e., large process noise covariance), then these estimators effectively perform least squares regression on the measured data. For unmodeled systems with noisy measurements, other system identification least squares methods [18] are reported. For periodically time-varying systems, frequency domain total least squares are proposed in [19], [20].

Other related work for sensor configuration in unknown environments is explored by [21], [22], which is based on an iterative process that identifies the optimal sensor configuration. However, these studies utilize a separate ego vehicle from the “sensor vehicles.” This approach is more appropriate for scenarios with a heterogeneous mix of vehicles such as a wheeled ego vehicle and UAV sensor vehicles.

The literature on wind estimation onboard UAVs largely addresses path- or trajectory tracking in the presence of wind disturbances [23]–[25], gust rejection for stability in cruise or hover conditions [26], [27], and/or dynamical modeling [28]. Wind estimation is studied in the airdrop literature [29] and in the study of weather systems [30].

The novelty of this work in relation to the literature is that we consider the wind estimation and package delivery problems simultaneously. The SUAVs are constrained to travel between a fixed initial point and a fixed destination, and do not travel any other special paths for estimating the wind. We explore strategies for reducing the total travel time of a team of SUAVs in unknown wind without modifying the path-planning algorithm from a typical minimum-cost approach. Therefore, the proposed method can be easily implemented with off-the-shelf SUAVs with little to no modification.

The rest of this paper is organized as follows. In Section II we introduce the main elements of the scenario(s) considered in this paper. In Section III, we describe the proposed method for estimating the unknown wind via data collected in SUAV passes. In Section IV, we provide numerical simulation results, and conclude the paper in Section V.

II. PROBLEM FORMULATION

Consider a 2D environment modeled by a directed graph $\mathcal{G} = (V, E)$. The vertex set V consists of uniformly spaced grid points in the environment. Let N_1 and N_2 denote the number of grid points along the x_1 and x_2 principal axes, respectively, in some prespecified Cartesian system. The edge set E consists of geometrically adjacent vertices as illustrated in Fig. 1. Adjacency is defined in the “4-neighbor” sense, i.e., grid points to the top, down, left, and right are considered adjacent, but diagonal adjacency is not considered. This assumption reflects the typical road network in an urban area. The vertices are labeled by integers, i.e., $V = \{1, 2, \dots, N_1 N_2\}$.

The distance along an edge $(i, j) \in E$ with $i, j \in V$ is denoted d_{ij} . The time-varying wind speed along edge (i, j) is denoted $w_{ij}(t)$, and it is assumed to be bounded $w_{ij}(t) \in [-w_{\max}, w_{\max}]$ and anti-symmetric $w_{ij}(t) = -w_{ji}(t)$ for all

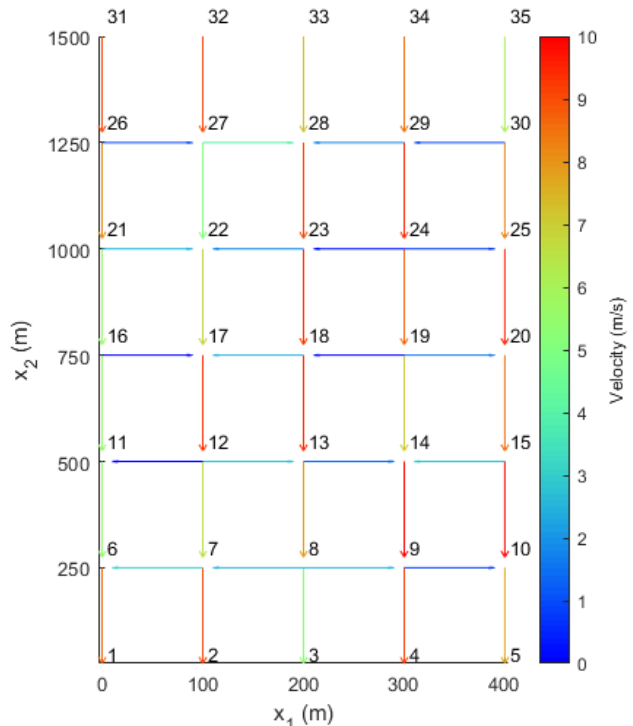


Fig. 1. Illustrative example of a wind field model on a 5×5 grid. Note that the top and bottom rows are only used as boundary conditions.

time $t \in \mathbb{R}_{\geq 0}$. The wind speed is assumed to be independent of the spatial variables x_1 and x_2 . The true values of $w_{ij}(t)$ are unknown to the SUAV team.

To estimate the wind speeds based on measurements, an underlying physics-based model is necessary. A high-fidelity fluid dynamical model is impractical for use in estimation, and therefore we postulate a simpler model, analogous to a simple electrical circuit. The wind speeds on each edge are assumed to be proportional to the spatial gradient of some (unknown) spatiotemporal “pressure” field denoted $P(x_1, x_2, t)$, analogous to a potential difference in electrical circuits. In this paper we assume $P_{x_1}(t) := \partial P / \partial x_1(t) = 0$, i.e., the only non-zero spatial gradients of the pressure field is $P_{x_2}(t) := \partial P / \partial x_2(t)$. In this paper, we focus on constant or time-periodic signals $P_{x_2}(t)$. The dependence of the wind speeds on this pressure gradient is as follows.

Edges along the x_2 direction are assumed to have fixed but unknown and strictly positive “resistance” values. Edges along the x_1 direction are assumed to have zero resistance values, due to which the edges along x_2 may be treated as parallel resistances in a circuit. These assumptions reflect typical Manhattan-type urban layouts with wide avenues in one direction and narrower roads connecting the wide avenues. With these assumptions the wind speeds on each edge can be easily calculated based on conservation of mass flow from one boundary of the environment to the other. Due to this model, we can transform the wind speed estimation problem as into the estimation of the signal

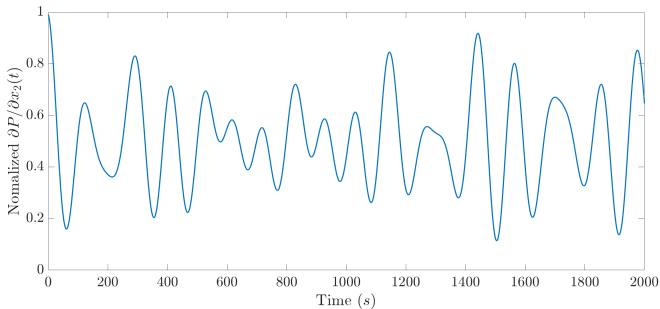


Fig. 2. An example of a periodic signal representing $P_{x_2}(t)$.

$P_{x_2}(t)$. Specifically, due to this model, it is easy to show that the wind speed on any edge $(i, j) \in E$ is proportional to the signal $P_{x_2}(t)$. We denote the constants of proportionality, which are unknown to the SUAVs, by ρ_{ij} .

An example wind field generated with this method is shown in Fig. 1. The first and last rows are used as non-traversable boundaries necessary to construct the field. In Fig. 1, the start is assumed to be the bottom left corner (vertex 6) and the goal is the top right corner (vertex 30), since we must omit the top and bottom rows of vertices. An example of the $P_{x_2}(t)$ considered is illustrated in Fig. 2, which is obtained by a weighted finite sum of sine and cosine signals (details in Section IV).

We assume that the measurements that each SUAV can make are of w_{ij} with additive measurement noise for the edges along which the SUAV travels. The measured wind speed is denoted by \tilde{w}_{ij} to distinguish from the true wind speed w_{ij} . Each SUAV travels at a fixed air-relative speed denoted u_0 .

III. METHOD

In what follows, \mathbb{Z} and \mathbb{R} are the sets of integers and real numbers, respectively. $\mathbb{E}[\cdot]$ denotes the expectation operator.

We consider a sequence of SUAV passes from the initial location to the destination. As previously mentioned, all data is stored and processed by a central agent. We neglect any issues related to the communication of data from the SUAVs to the agent. The agent's computations are in discrete time, which we denote by integers k, m, n , etc. to indicate time instants t_k, t_m, t_n , etc. Successive discrete time instants are all separated by a uniform and fixed time step of Δt . The sequence of all time instants in succession in an interval from n to m with $n, m \in \mathbb{Z}$ and $n < m$ is denoted by $n : m$.

The agent maintains an estimate of the transition cost, denoted c_{ij} , for each edge $(i, j) \in E$. Because we are interested in minimum-time travel, the transition cost of an edge is equal to the time taken to travel along that edge. Before the first pass, when no wind speed data are available, the cost estimates for all edges are uniformly initialized to

$$c_{ij} = d_{ij}(u_0 + w_{\max})^{-1}, \quad \text{for each } (i, j) \in E. \quad (1)$$

This initialization is “optimistic” in that it assumes the highest possible tailwind along each edge, and is therefore a lower bound on the true edge cost. Note that this optimistic

initialization disregards the anti-symmetric property of wind speeds on edges.

For each pass, the agent plans the minimum-time path for the SUAV. This is easily achieved by executing Dijkstra's algorithm on the graph \mathcal{G} using the most recent estimates of the costs c_{ij} . Due to the optimistic initialization in (1), in the first few passes there may be several paths with equal cost, of which one is randomly chosen. This may be accomplished within Dijkstra's algorithm itself at the crucial step of popping the fringe (also known as the “open” list), i.e., choosing the vertex-label pair with minimum label.

The SUAV then traverses this planned path, i.e., executes the pass. Consider an edge $(i, j) \in E$ traversed within this pass, and denote by $n, m \in \mathbb{Z}$ the discrete time instants at which the SUAV enters and exits this edge, respectively. During this traversal, the SUAV measures and provides to the agent the wind speed time series $\tilde{w}_{ij}(n : m)$. The agent's objective then is to use these measurements to update the edge cost estimates.

To this end, we consider four different cases as follows:

- Case 1: The true wind speed w_{ij} is time-invariant for each $(i, j) \in E$ and there is no measurement noise, i.e., $\tilde{w}_{ij} = w_{ij}$.
- Case 2: The true wind speed w_{ij} is time-invariant for each $(i, j) \in E$ and there is zero-mean measurement noise, i.e., $\mathbb{E}[\tilde{w}_{ij} - w_{ij}] = 0$.
- Case 3: The true wind speed w_{ij} is time-varying for each $(i, j) \in E$ and there is no measurement noise, i.e., $\tilde{w}_{ij}(k) = w_{ij}(k)$ for each $k \in \mathbb{Z}$.
- Case 4: The true wind speed w_{ij} is time-invariant for each $(i, j) \in E$ and there is zero-mean measurement noise, i.e., $\mathbb{E}[\tilde{w}_{ij}(k) - w_{ij}(k)] = 0$ for each $k \in \mathbb{Z}$.

A. Edge Cost Estimates

The agent's method of updating the edge cost estimates differs for each of the aforesaid Cases. For Case 1, the edge costs may be updated simply by considering the SUAV's time of travel along the edge (i, j) in relation to the (known) distance d_{ij} of travel. Specifically, the agent updates c_{ij} as

$$c_{ij} = d_{ij}(u_0 + \tilde{w}_{ij})^{-1}. \quad (2)$$

For Case 2, where zero mean measurement noise is present, the agent updates the edge costs by considering the mean value of the measured wind speeds, i.e.,

$$c_{ij} = d_{ij} \left(u_0 + \frac{1}{m-n} \sum_{k=n}^m \tilde{w}_{ij}(k) \right)^{-1}. \quad (3)$$

For Cases 3 and 4, where the wind speeds are time-varying, the following crucial problem arises. The observations of the wind speeds are restricted to the time window $n : m$ during which an SUAV traverses the edge. Furthermore, because the edge “resistance” values are different, when the SUAV transitions from one edge to the next, there is in general a discontinuity in the measured wind speed. For example, suppose (i, j) and (j, ℓ) are successive edges in the SUAV's path. The SUAV completes traveling along

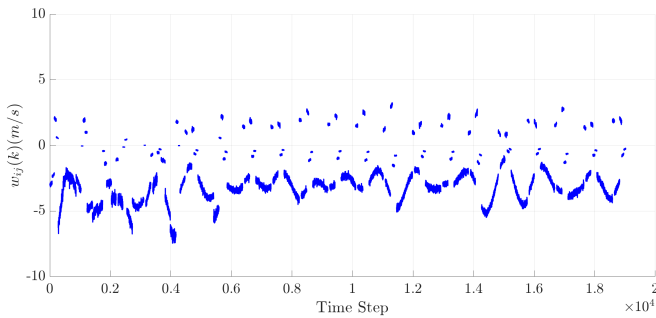


Fig. 3. Raw $\tilde{w}_{ij}(k)$ measurement data for a simulated Case 3 on the 5×5 grid shown in Fig. 1.

(i, j) at time m and starts to traverse edge (j, ℓ) at time $m + 1$. In general there will be a discontinuity such that $|\tilde{w}_{ij}(m) - \tilde{w}_{j\ell}(m + 1)|$ cannot be guaranteed to be smaller than some ε dependent on the time step Δt .

Figure 3 illustrates the (noiseless) measurements of wind speeds along edges a numerical simulation of Case 3 and these discontinuities are clearly visible. The presence of these discontinuities makes the time-series estimation of wind speeds and, consequently, the edge costs, nontrivial. To resolve this issue, we focus instead on the estimation of the time-series $P_{x_2}(k)$, which is continuous.

Based on the model postulated in Section II, recall that the wind speed along each edge is proportional to the pressure gradient $P_{x_2}(k)$:

$$w_{ij}(n : m) = \varrho_{ij} P_{x_2}(n : m). \quad (4)$$

Let $\hat{P}_{x_2}(n : m)$ denote the mean value of an estimate of $P_{x_2}(n : m)$. We may then approximate the unknown constant ϱ_{ij} using the time-averaged values of the measured wind speed and of the estimate \hat{P}_{x_2} as:

$$\varrho_{ij} = \frac{1}{m - n} \left(\sum_{k=n}^m \tilde{w}_{ij}(n : m) \right) \left(\sum_{k=n}^m \hat{P}_{x_2}(n : m) \right)^{-1}. \quad (5)$$

The agent can then approximate the edge cost for edge (i, j) by an expression similar to (6):

$$c_{ij} = d_{ij} (u_0 + \varrho_{ij})^{-1}. \quad (6)$$

Note that this is a static (time-invariant) approximation of the edge cost, which in principle will be time-varying when the wind speeds are time-varying. Searching a graph with time-varying edge costs can significantly worsen computational complexity.

Based on (4)–(5), we focus on the problem of finding the estimate $P_{x_2}(k)$ in Cases 3 and 4, namely, where measurement noise is either absent or is of zero mean.

B. $P_{x_2}(k)$ Estimation

For Cases 3 and 4, we consider first a simple least-squares polynomial estimate for $P_{x_2}(k)$. To this end, the agent maintains a time series $w : \mathbb{Z} \rightarrow \mathbb{R}$ that “stitches” the time-window measurements $\tilde{w}_{ij}(n : m)$ into a single time series

that extends over all SUAV passes. This stitching is achieved by scaling the values of the new window of measurements to the larger time series, followed by concatenation. The desired signal $\hat{P}_{x_2}(k)$ is then recovered by normalizing w . Specifically, we concatenate $w(1 : n - 1)$ with the new measurements by

$$w(n : m) := r \tilde{w}_{ij}(n : m),$$

where $r := (\tilde{w}_{ij}(n))^{-1} (w(n - 1) + \dot{w}(n - 1) \Delta t)$ is a scaling factor. The value of the derivative $\dot{w}(n - 1)$ is calculated numerically using a second-order backward difference approximation. Finally, we normalize the concatenated time series to find

$$\hat{P}_{x_2}(1 : m) := \frac{w(1 : m)}{\max_{k \in [1, m]} |w(k)|}.$$

Whereas this method suffices for Case 3 (no measurement noise), the numerical derivative calculation obviously fails for Case 4. In this Case, we may use a polynomial approximation of $\tilde{w}_{ij}(n : m)$. To avoid overfitting, we consider a quadratic polynomial. Let $\hat{w}_{ij}(k)$ denote a quadratic least-squares approximation to the measured signal $\tilde{w}_{ij}(n : m)$. Then, we redefine the aforesaid scale factor as

$$r := (\hat{w}_{ij}(n - \frac{1}{2}))^{-1} w(n - \frac{1}{2}),$$

while the rest of the calculations remain similar.

The advantage of the method discussed so far is that we make no assumptions about the nature of the signal $P_{x_2}(t)$ other than it is once-differentiable with respect to time. The shortcoming of this method is that, in the presence of measurement noise, the error propagates and grows over time. Therefore, we develop a Kalman filter, while noting a restriction of its applicability to a specific class of signals.

Consider a state variable of the form

$$\mathbf{x} = (y_1, y_2, \dots, y_N, \dot{y}_1, \dot{y}_2, \dots, \dot{y}_N, \ddot{y}_1, \ddot{y}_2, \dots, \ddot{y}_N),$$

where $y_N(t) = P_{x_2}(t)$ and y_1, \dots, y_{N-1} are hidden variables. We write a state evolution model and observation model of the form

$$\mathbf{x}(k) = A \mathbf{x}(k - 1) + \boldsymbol{\eta}_1(k - 1), \quad (7)$$

$$\mathbf{z}(k) = C \mathbf{x}(k) + \boldsymbol{\eta}_2(k), \quad (8)$$

where $\boldsymbol{\eta}_1$ and $\boldsymbol{\eta}_2$ are zero mean Gaussian white noise processes with error covariances Q and R , respectively.

The hidden variables may be thought of as displacements of a series of N fictitious mass-spring systems. Without damping, we focus on the modeling of periodic signals that are exactly expressed by an N -term Fourier series expansion.

Stated differently, we may perform a fast Fourier transform (FFT) analysis on a historical dataset of $P_{x_2}(k)$ or on the data collected during passes to find the N most dominant frequency components, their amplitudes, and phase shifts.

In this model, we write the A matrix as

$$\begin{aligned}
A_{1:2N,1:3N} &= \begin{bmatrix} 1 & 0 & \dots & \Delta t & 0 & \dots & 0 \\ 0 & 1 & 0 & \dots & \Delta t & 0 & 0 \\ \vdots & 0 & 1 & 0 & \dots & \Delta t & 0 \\ \vdots & \vdots & \ddots & \ddots & \ddots & \dots & \ddots \end{bmatrix}, \\
A_{2M+1:3N,1:N} &= \begin{bmatrix} -(K_1 + K_2) & K_2 & 0 & \dots & 0 \\ -K_2 & -(K_2 + K_3) & K_3 & 0 & 0 \\ 0 & \ddots & \ddots & \ddots & 0 \\ 0 & \dots & 0 & K_{N-1} & -K_N \end{bmatrix}, \\
A_{2N+1:3N,2N+1:3N} &= 0, \\
C &= [0 \quad \dots \quad 1 \quad 0 \quad \dots \quad 0].
\end{aligned} \tag{9}$$

Here the constants K_ℓ are the fictitious spring stiffness values and these are equal to the square roots of the frequencies resulting from the FFT analysis mentioned above.

The amplitude and phase data extracted from the FFT can be used to set a prior mean $\hat{x}(0)$ and error covariance $\mathcal{P}(0)$ for the Kalman filter. Whereas the covariance R may be determined from measurement error calibration, the covariance Q must be tuned based on the observed innovations (residual error) sequence. This is because the FFT analysis can provide inaccurate frequency information with small time windows. One strategy for tuning Q is to set large diagonal values during the early passes and then tuning it based on the FFT analysis after sufficient time has passed.

IV. RESULTS AND DISCUSSION

A. Numerical Simulation Setup

In this section, we report the results of numerical simulation studies of the proposed method. Inspired by the city blocks in Manhattan, (New York City, NY, USA) between the Hudson River and Central Park area, a directional graph model of the city roadways is produced, as illustrated in Fig. 1. This model considers uniform road lengths of 100 and 250 meters along the x_1 and x_2 directions, respectively. Winds speeds are calculated per the pressure gradient model postulated in Section II and all wind speeds are scaled such that the maximum speed is equal to a globally defined maximum of $w_{\max} = 10$ m/s. The air-relative speed of each SUAV is fixed at $u_0 = 15$ m/s.

In the context of the pressure gradient model postulated in Section II, all edge resistances are fixed at arbitrarily chosen values in $[0.5, 1]$. The ground truth pressure gradient $P_{x_2}(t)$ signal is produced via the following expression including noise:

$$P_{x_2}(t) = d_0 + \sum_{\ell=1}^N a_\ell \cos(2\pi b_\ell t + c_\ell) + v(t) \tag{10}$$

TABLE I
SEQUENTIAL TRIALS UNTIL OPTIMAL PATH CONVERGENCE

	Case 1	Case 2	Case 3	Case 4
5x5	6	6	6	7
7x7	12	12	12	14
9x9	15	16	15	18

where a_ℓ , b_ℓ , and c_ℓ are the amplitude, frequency, and phase respectively of each periodic component in the series, $v(t)$ simulates the measurement noise, and d_0 is a constant.

For repeated simulation trials, we need to randomly produce a ground truth signal $P_{x_2}(t)$ with normalized values such that $P_{x_2}(t) \in [0, 1]$. To this end, d_0 is set to 0.5. The amplitude coefficients a_ℓ are obtained by sampling a uniform distribution over $[0, 1]$ and then normalized as

$$a_\ell = \frac{1}{2} a_{\bar{\ell}} \left(\sum_{\bar{\ell}=1}^N a_{\bar{\ell}} \right)^{-1}.$$

Similarly, the frequency coefficients b_ℓ are obtained by sampling a uniform distribution over some finite frequency range of the user's choice. The phase coefficients c_ℓ are sampled from a uniform distribution over $[0, 2\pi]$.

For Cases 3 and 4, $N = 6$ terms were used to produce ground truths $P_{x_2}(t)$ via (10). The frequency terms were chosen randomly between 300s^{-1} and 500s^{-1} . A sample P_{x_2} is shown in Fig. 2. For Cases 2 and 4, the noise term was simulated as $v(k) \sim \mathcal{N}(0, 0.025)$.

B. Performance Analysis

Because each pass is assumed to be conducted along a minimum-time path, per the cost estimates available immediately before the pass, the main performance metric of interest is the number of passes needed until the optimal path is found. We record also the time of travel for each pass as a measure of performance, but this measure is dependent on various dimensional assumptions, e.g., edge length, maximum wind speed, etc.

Table I shows the number of passes until the optimal path was found, i.e., no other paths of lower cost were found in subsequent passes. Figures 4–5 show an example of the evolution of the incurred and expected path costs for each pass for Cases 1 and 3 respectively on a 9×9 grid. The incurred cost is higher in the first few passes because the edge cost estimates are initialized optimistically, as discussed in Section III.

When the true optimal path is taken, the expected data point is marked with a circle. In these examples, the optimal path is found after the 15th pass and no other path is selected for future passes. Therefore, 15 is recorded in Table I.

For Case 1, the expected and incurred costs are equal once the optimal path is reached. This is not true for Cases 2–4 due to measurement noise and estimation errors. The number of passes required for Case 1 (no measurement noise and constant P_{x_2}) is a lower bound for the number of passes required for any of the other cases. Table I demonstrates that

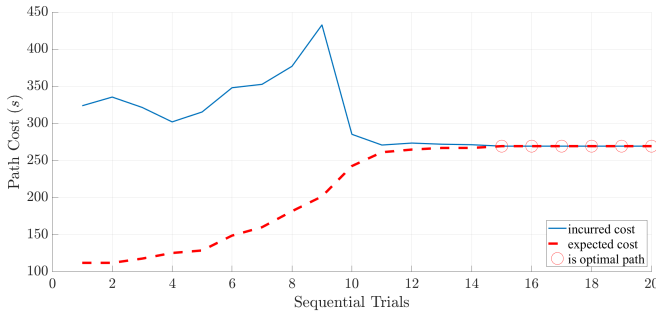


Fig. 4. Expected vs incurred path cost for a 9×9 grid, environment Case 1.

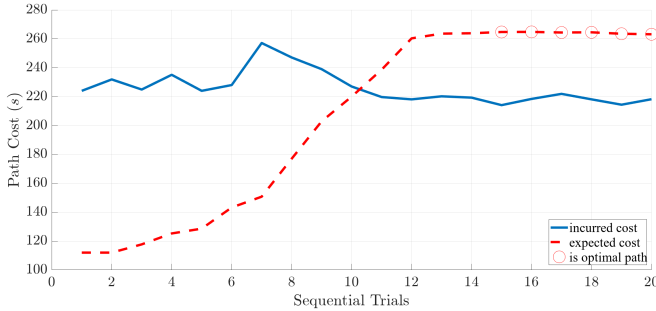


Fig. 5. Expected vs incurred path cost for a 9×9 grid, environment Case 3.

the proposed wind speed and edge cost estimation method converges to the optimal path with the minimum or near-minimum number of passes for Cases 2–4 as well, regardless of grid size.

For Cases 2 and 4, the number of passes required to find the optimal path depends on the signal to noise ratio in $P_{x_2}(t)$. For Case 4, the problem of error prorogation due to the polynomial curve fit (see Section III) becomes prominent. Figures 6–7 show that the steady state error can be reduced by applying a Kalman Filter to estimate $P_{x_2}(t)$.

The Kalman Filter can suffer from high errors early in the signal while the input data window is too small for the FFT. This does not alter performance since c_{ij} is determined using the most recent measurements $\tilde{w}_{ij}(n : m)$ available, which are then used to estimate q_{ij} by (5).

Once the optimal path is found, the Kalman Filter better

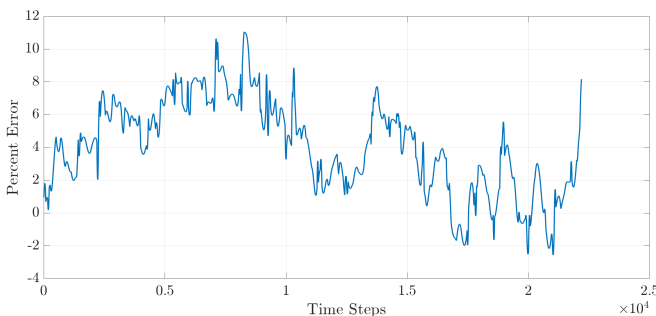


Fig. 6. Percent error between the estimated and true $P_{x_2}(t)$ for a 5×5 grid, Case 4 without a Kalman Filter.

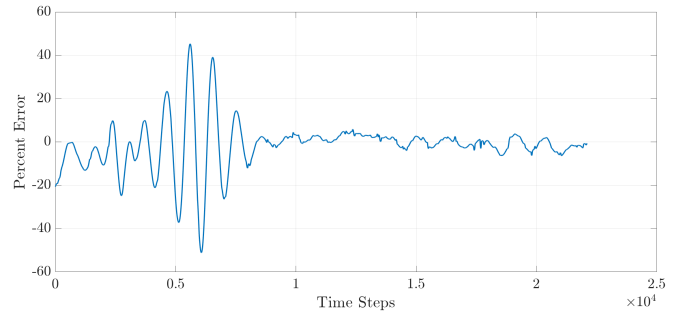


Fig. 7. Percent error between the estimated and true $P_{x_2}(t)$ for a 5×5 grid, Case 4 with a Kalman Filter.

approximates $P_{x_2}(n : m)$ as n gets large since it is less prone to propagating errors. However, using the Kalman filter did not lead to the optimal path in fewer passes than the polynomial curve fit-based estimation alone.

V. CONCLUSIONS

We studied the problem of planning the paths of a team of UAVs sequentially flying from a fixed initial point to a fixed destination in an unknown wind field. The novel aspect of our problem formulation is that each UAV measures wind speeds while traversing along a minimum-cost path planned based on the current wind field estimate. We provided a technique of estimating the wind field such that the optimal (minimum-time) path is found after a small number of passes. We considered cases of static and periodically time-varying winds with and without measurement noise. The number of passes required for the easiest case (static wind, no measurement noise) is the minimum required for all other cases. We demonstrated numerical simulation results where optimal paths were found for all other cases with a minimum or near-minimum number of passes. Future work will expand the problem to multiple UAVs running concurrently and a simulation with high-fidelity flow fields and UAV flight dynamics.

REFERENCES

- [1] A. P. Cohen, S. A. Shaheen, and E. M. Farrar, “Urban air mobility: History, ecosystem, market potential, and challenges,” *IEEE Transactions on Intelligent Transportation Systems*, vol. 22, no. 9, pp. 6074–6087, 2021.
- [2] B. Zhao, Y. Suo, L. Tang, C. Li, M. Fu, and L. Huang, “Urban air mobility for time-sensitive goods with explicit customer preferences: A case study on chengdu,” *Journal of Air Transport Management*, vol. 118, p. 102613, 2024.
- [3] R. Goyal, C. Reiche, C. Fernando, J. Serrao, S. Kimmel, A. Cohen, and S. Shaheen, “Urban air mobility (uam) market study,” Tech. Rep. HQ-E-DAA-TN65181, 2018. Available: <https://ntrs.nasa.gov/citations/20190001472>.
- [4] M. Rakib, S. Evans, and P. Clausen, “Measured gust events in the urban environment, a comparison with the iec standard,” *Renewable Energy*, vol. 146, pp. 1134–1142, 2020.
- [5] M. Chrit, “Reconstructing urban wind flows for urban air mobility using reduced-order data assimilation,” *Theoretical and Applied Mechanics Letters*, vol. 13, no. 4, p. 100451, 2023.
- [6] M. Xue and M. Wei, *Small UAV Flight Planning in Urban Environments*.
- [7] J. Wu, Y. Ye, and J. Du, “Multi-objective reinforcement learning for autonomous drone navigation in urban areas with wind zones,” *Automation in Construction*, vol. 158, p. 105253, 2024.

- [8] Korprasertsak, Natapol and Leephakpreeda, Thananchai, "Improving accuracy of wind analysis with multiple sampling rates of wind measurement," *E3S Web Conf.*, vol. 95, p. 02002, 2019.
- [9] S. M. Lavalle, *Planning Algorithms*. Cambridge University Press, 2006.
- [10] B. K. Patle, G. B. L. A. Pandey, D. R. Parhi, and A. Jagadeesh, "A review: On path planning strategies for navigation of mobile robot," *Defence Technology*, vol. 15, pp. 582–606, August 2019.
- [11] T. Wen, X. Wang, Z. Zheng, and Z. Sun, "A DRL-based path planning method for wheeled mobile robots in unknown environments," *Computers and Electrical Engineering*, vol. 118, p. 109425, 2024.
- [12] Y. Qin, Z. Zhang, X. Li, W. Huangfu, and H. Zhang, "Deep reinforcement learning based resource allocation and trajectory planning in integrated sensing and communications UAV network," *IEEE Transactions on Wireless Communications*, vol. 22, no. 11, pp. 8158–8169, 2023.
- [13] F. L. Lewis, L. Xie, and D. Popa, *Optimal and robust estimation: with an introduction to stochastic control theory*. CRC press, 2017.
- [14] I. J. Myung, "Tutorial on maximum likelihood estimation," *Journal of mathematical Psychology*, vol. 47, no. 1, pp. 90–100, 2003.
- [15] S. Thrun, W. Burgard, and D. Fox, *Probabilistic Robotics*. The MIT Press, 2006.
- [16] S. J. Julier and J. K. Uhlmann, "Unscented filtering and nonlinear estimation," in *Proceedings of the IEEE*, vol. 92, pp. 401–422, Mar. 2004.
- [17] X. Deng, A. Mousavian, Y. Xiang, F. Xia, T. Bretl, and D. Fox, "Poserbpf: A rao-blackwellized particle filter for 6-d object pose tracking," *IEEE Transactions on Robotics*, vol. 37, no. 5, pp. 1328–1342, 2021.
- [18] C. Heij and W. Scherrer, "Consistency of system identification by global total least squares," *Automatica*, vol. 35, no. 6, pp. 993–1008, 1999.
- [19] E. Louarroudi, J. Lataire, and R. Pintelon, "Frequency domain total least squares identification of linear, periodically time-varying systems from noisy input-output data," *IFAC Proceedings Volumes*, vol. 44, no. 1, pp. 13115–13120, 2011. 18th IFAC World Congress.
- [20] G. Liu, M. li Yu, L. Wang, Z. yi Yin, J. ke Liu, and Z. rong Lu, "Rapid parameter identification of linear time-delay system from noisy frequency domain data," *Applied Mathematical Modelling*, vol. 83, pp. 736–753, 2020.
- [21] P. Poudel and R. V. Cowlagi, "Coupled sensor configuration and planning in unknown dynamic environments with context-relevant mutual information-based sensor placement," in *2024 American Control Conference (ACC)*, pp. 306–311, IEEE, 2024.
- [22] P. Poudel and R. V. Cowlagi, "Reconfiguration costs in coupled sensor configuration and path-planning for dynamic environments," in *AIAA Scitech 2025 Forum*, (Orlando, Florida), 6-10 January 2025. to appear.
- [23] I. Sarras and H. Siguerdidjane, "On the guidance of a uav under unknown wind disturbances," in *2014 IEEE Conference on Control Applications (CCA)*, pp. 820–825, IEEE, 2014.
- [24] B. Zhou, H. Satyavada, and S. Baldi, "Adaptive path following for unmanned aerial vehicles in time-varying unknown wind environments," in *2017 American Control Conference (ACC)*, pp. 1127–1132, 2017.
- [25] J. Yang, C. Liu, M. Coombes, Y. Yan, and W.-H. Chen, "Optimal path following for small fixed-wing uavs under wind disturbances," *IEEE Transactions on Control Systems Technology*, vol. 29, no. 3, pp. 996–1008, 2021.
- [26] Z. Xing, Y. Zhang, and C.-Y. Su, "Active wind rejection control for a quadrotor uav against unknown winds," *IEEE Transactions on Aerospace and Electronic Systems*, vol. 59, no. 6, pp. 8956–8968, 2023.
- [27] C. Liu and W.-H. Chen, "Disturbance rejection flight control for small fixed-wing unmanned aerial vehicles," *Journal of Guidance, Control, and Dynamics*, vol. 39, no. 12, pp. 2810–2819, 2016.
- [28] B. H. Wang, D. B. Wang, Z. A. Ali, B. T. Ting, and H. Wang, "An overview of various kinds of wind effects on unmanned aerial vehicle," *Measurement and Control*, vol. 52, no. 7-8, pp. 731–739, 2019.
- [29] M. R. Cacan, E. Scheuermann, M. Ward, M. Costello, and N. Slegers, "Autonomous airdrop systems employing ground wind measurements for improved landing accuracy," *IEEE/ASME Transactions on Mechatronics*, vol. 20, no. 6, pp. 3060–3070, 2015.
- [30] D. J. Cecil and S. K. Biswas, "Hurricane imaging radiometer (hirad) wind speed retrievals and validation using dropsondes," *Journal of atmospheric and oceanic technology*, vol. 34, no. 8, pp. 1837–1851, 2017.